Neoplasma 2023; 70(3): 390–401

doi:10.4149/neo_2023_230525N283

Effects of different-sized silver nanoparticles on morphological and functional alterations in lung cancer and non-cancer lung cells

Kristina JAKIC[1], Michal SELC[1,2], Radka MACOVA[1], Antonia KURILLOVA[3], Libor KVITEK[3], Ales PANACEK[3,*], Andrea BABELOVA[1,2,*]

[1]Department of Nanobiology, Cancer Research Institute, Biomedical Research Center, Slovak Academy of Sciences, Bratislava, Slovakia; [2]Centre for Advanced Material Application, Slovak Academy of Sciences, Bratislava, Slovakia; [3]Department of Physical Chemistry, Faculty of Science, Palacky University in Olomouc, Olomouc, Czech Republic

**Correspondence: andrea.babelova@savba.sk; ales.panacek@upol.cz*

Received May 25, 2023 / Accepted June 22, 2023

Silver nanoparticles (AgNPs) exhibit unique physicochemical properties, making these nanomaterials attractive for various medical applications. Among them, AgNPs have shown great potential in the treatment of cancer by inducing apoptosis in cancer cells, inhibiting tumor growth, and enhancing the efficacy of conventional cancer treatments such as chemotherapy and radiation therapy. Despite the promising therapeutical advantage of AgNPs, there are several challenges that need to be addressed. One of the most important is AgNPs' toxicity, which in case of treatment might be extended to non-cancerous cells and tissues. In our study, we therefore investigated the effects of spherical AgNPs with the silver core size of 10, 30, and 45 nm coated with polyacrylic acid (PAA-AgNPs) in an in vitro model using cancer (A549) and non-cancer (HEL299) cells. We estimated the impact of these nanoparticles on cell viability, cell proliferation, and cell actin cytoskeleton remodeling. Moreover, changes in the expression of *TNFA*, *IL-10*, *FN1*, and *SOD1* mRNA induced by PAA-AgNPs were determined. Our results suggest that the smallest (10 nm) PAA-AgNPs are the most effective in apoptosis induction, however, they are also the most toxic from the three AgNPs types to both, cancer and non-cancer cells, while bigger (30 and 45 nm) PAA-AgNPs showed fewer undesirable effects in these pulmonary cells.

Key words: AgNPs; lung cancer; A549; HEL299; polyacrylic acid

Nanotechnologies offering particles in the nanoscale range are predetermined for applications in medicine [1, 2]. To make this vision successful and safe for a patient, it is necessary to understand how nanoparticles behave in the living organism and how living organisms respond to the nanoparticles. Lungs, as major organs of the respiratory system with their air-blood barrier, represent a direct connection between the inhaled air and the alveoli enabling gas exchange. An important link between the oxygen-containing atmosphere and the working tissues consuming oxygen is blood circulation sending blood to the lungs to become oxygenated. This might be one of the reasons why lungs belong to organs with considerable nanoparticle accumulation [3]. Nanoparticles delivered to the lung may increase the activity of factors mediating inflammatory and fibrogenic processes [4, 5]. For regulation of the inflammatory processes within the lung, counterplay between *TNFA* (tumor necrosis factor alpha) as a master proinflammatory cytokine and *IL-10* (interleukin 10) as its inhibitor has been identified as an essential part of the pulmonary immune response [6]. The toxicity of AgNPs has been mainly attributed to the reactive oxygen species induction in eukaryotic cells [7], however these mechanisms are to be confirmed in mammalian cells [8]. Nevertheless, an increase in *SOD1* (superoxide dismutase 1) and *SOD2* (superoxide dismutase 2) has been detected in cerebral myelin as a consequence of AgNPs exposure confirming oxidative stress a mechanism of AgNPs-induced neurotoxicity [9]. On the other hand, nanomaterials are being engineered to serve medical purposes including therapies for pulmonary diseases [10, 11]. Nanoparticles from noble metals gained great attention thanks to their photothermal and optical properties, which allow for simultaneous diagnostic and therapeutic possibilities [12]. An attractive group of engineered nanomaterials is antimicrobial agents combating infections, with silver nanoparticles (AgNPs) as a leading nanomaterial type [13, 14]. Thanks to the excellent antibiotic activity of AgNPs, they are added to a number of medical devices including implants, dressings, surgical tools, catheters, prosthetic devices, and

dental products [15, 16]. Due to their unique physicochemical properties, also the use of AgNPs for targeted drug delivery and imaging for the diagnosis and treatment of cancer has been intensively investigated [17–20]. Concerning lung cancer, AgNPs have been shown to inhibit the growth of lung cancer cells and the growth of lung xenograft tumors in immunodeficient mice [21]. The newest research reveals that the anticancer effect of AgNPs on lung cancer cells may lie in the enhancement of apoptosis in these cells [22]. To follow the progress of anticancer approaches to lung cancer, the effects of AgNPs on non-cancer lung cells should be recognized on the background of their action towards cancer cells. In line with this, the aim of this study was to estimate the biological effects of AgNPs with different core sizes (10 nm-PAA-AgNPs(10), 30 nm-PAA-AgNPs(30), 45 nm-PAA-AgNPs(45)) coated with polyacrylic acid (PAA) on cancer (A549) and non-cancer (HEL299) pulmonary cells *in vitro*. We have estimated the cytotoxicity of PAA-AgNPs, effects on the proliferation activity of cells, impact on cell cycle, as well as nanoparticle-induced mRNA expression, and compared these effects in both A549 and HEL299 cell lines. Short- (5 h) and long- term (24 h) exposure was investigated in order to detect early as well as later PAA-AgNPs-induced *TNFA*, *IL-10*, *FN1* (fibronectin), and *SOD1* mRNA expression. Eventually, the stability of the actin cytoskeleton after PAA-AgNPs exposure has been compared between A549 and HEL299 cells.

Materials and methods

Cell culture and cultivation. The human lung adenocarcinoma epithelial A549 (ATCC® CCL-185™) cells were cultivated in DMEM low glucose medium supplemented with 10% FBS and 1% penicillin-streptomycin. HEL299 (CLS #300193), human embryo lung cells, were cultivated in MEM supplemented with 10% FBS, 1% penicillin-streptomycin, 1% non-essential amino acids, and 1% sodium pyruvate. Both cell cultures were maintained in a sterile humidified incubator (5% CO_2, 37 °C). All media and supplements were from Gibco.

Synthesis of AgNPs with various sizes. For the synthesis of AgNPs stabilized by polyacrylic acid, silver nitrate (99.9%, Sigma-Aldrich), ammonia (p.a., 27% [w/w] aqueous solution, Sigma-Aldrich), sodium hydroxide (p.a., Lachema, Czech Republic), polyacrylic acid (PAA, M.W.100 000; 35% (w/w) aqueous solution, Sigma Aldrich), D-(+)-maltose monohydrate (p.a., Sigma-Aldrich), and $NaBH_4$ (p.a., Sigma-Aldrich) were used without further purification. The solutions were prepared using deionized water (18 MΩ·cm, Millipore). PAA-AgNPs were synthesized according to a previously reported procedure using a Tollens reaction with slight modification in PAA concentration [23]. The Tollens reaction consists of the reduction of the complex cation $[Ag(NH_3)_2]^+$ by D-maltose in an alkaline medium. The reaction mixture was prepared by the addition of $AgNO_3$ and NH_3 solutions at final concentrations of 10^{-3} mol/l and 5×10^{-3} mol/l, respectively. After that, pH of the reaction system was adjusted to 11 by the addition of NaOH solution at a final concentration of 0.01 mol/l. The reduction was initiated by the addition of maltose (0.01 mol/l final concentration). AgNPs with various sizes of 30 nm and 45 nm were prepared by the modification of the aforementioned Tollens process by the addition of a long-chain PAA into the reaction mixture. The PAA solution was added before the addition of the maltose at desired volume to achieve the final PAA concentrations of 10^{-10} mol/l for 30 nm sized PAA-AgNPs and 2.5×10^{-9} mol/l for 45 nm sized PAA-AgNPs. The final and stable pH of the prepared silver colloids was 10.5 (for 10^{-10} mol/l PAA) and 10 (for 2.5×10^{-9} mol/l PAA), respectively.

In the case of the synthesis of 10 nm sized PAA-AgNPs, the strong reducing agent $NaBH_4$ was used instead of maltose. The final concentration of $AgNO_3$ and NH_3 was the same and the final concentration of PAA was 2.5×10^{-9} mol/l. No NaOH solution had to be added to the reaction system and the final and stable pH of the reaction mixture was 8. The reaction was initiated by the rapid addition of $NaBH_4$ solution at a final concentration of 10^{-3} mol/l. All AgNP syntheses were performed at laboratory temperature (~25 °C), under vigorous stirring. All the PAA-AgNPs colloids were characterized and used for cytotoxicity evaluations in the form as they were synthesized. The average sizes and size distributions of the prepared AgNPs were determined by dynamic light scattering (DLS) using the Zetasizer Nano ZS (Malvern). The nanodimensions of the synthesized AgNPs were confirmed by transmission electron microscopy using the JEM-2010 (Jeol) and by UV-Vis absorption spectroscopy with the Specord S 600 spectrophotometer (Analytik Jena AG). For UV-Vis spectroscopy measurements, silver colloids were 10 times diluted with distilled water.

MTT. A549 or HEL299 cells (1×10^4 and 2×10^4 cells/well, respectively) were seeded onto the 96-well plate in a serum-free medium for 16 hours. The medium was then replaced with a 2% FBS medium containing AgNPs at the defined concentrations. After 24 h incubation with AgNPs, the medium was replaced with 150 µl of a medium containing 0.5 mg/ml 3-(4,5-dimethylthiazol-2-yl)-2,5-diphenyltetrazolium bromide (MTT; Sigma-Aldrich). After 3 h, formazan crystals were dissolved with 100 µl of dimethyl sulfoxide (Centralchem) and absorbance was measured at 540 nm on X-mark (Bio-Rad).

Proliferation assay. A549 or HEL299 cells (5×10^3 and 1×10^4 cells/well, respectively) were seeded onto the 96-well plate in a 10% FBS medium containing AgNPs for 48 h. Every 30 min, the confluency was measured using a live cell analyzer Juli-FL (NanoEnTek).

Apoptosis and cell cycle analysis. A549 or HEL299 cells (2×10^5 and 3×10^5 cells/well, respectively) were seeded onto the 6-well plate in a serum-free medium for 6 h and then incubated with 10% medium containing AgNPs at the defined concentrations for 24 h. Cells were trypsinized, centrifuged for 5 min at 250×*g*, and washed with ice-cold PBS. Pellet was

divided into two equal parts for measurement of apoptosis and cell cycle. For apoptosis, samples were processed using a kit CF®488A Annexin V and PI Apoptosis Kit (Biotium). For the cell cycle, cells were incubated with Triton-X100 and 0.5 mg/ml RNase A (Sigma-Aldrich) in the dark for 20 min at 37 °C, then 6 μg/ml propidium iodide (Sigma-Aldrich) was added. The cell cycle was analyzed using the BD FACSCanto™ II flow cytometry system (BD Biosciences) and evaluated using FCS Express software (De Novo Software).

PCR. A549 or HEL299 cells (3×10^5 cells/well) were seeded onto the 6-well plate in a serum-free medium for 6 h and then incubated with a 10% medium containing AgNPs at the defined concentrations for 5 h and 24 h. Total RNA was isolated using TRIreagent (Sigma), residual DNA was removed by using DNase I, RNase-free (Thermo Scientific™), and RNA was transcribed into the cDNA using the RevertAid First Strand cDNA Synthesis Kit (Thermo Scientific™). Real-time PCR was performed using ampliTune® qPCR EvaGreen® Mix (Selecta Biotech SE) in an AriaMx real-time PCR cycler (Agilent). Primer sequences used are listed in Table 1. Gene expression was calculated using the $2^{-\Delta\Delta CT}$ method.

Immunocytochemistry. Cells (HEL299 or A549) were seeded onto 10 mm cover glasses (4×10^4 cells/glass). After incubation with nanoparticles for 24 h, cells were washed with PBS and fixed with 4% paraformaldehyde for 15 min. The cytoskeleton of the cells was stained with Phalloidin Alexa Fluor 546 conjugated antibody (Cat. No. A22283, Life Technologies) and nuclei were counterstained with DAPI. For the analysis of the cell actin cytoskeleton, a fluorescence microscope (MetaSystems, Alogo, Ltd.) with Zeiss Axio Imager.Z2 and ISIS software were used. Measurements were analyzed using ImageJ software.

Statistical analysis. At least three independent experiments (N=3) performed in duplicates (n=6) were used to determine the statistical significance in this study. The Shapiro-Wilk test was used to determine normal distribution. In a normal distribution, an unpaired t-test was used to determine the statistical significance. The nonparametric Mann-Whitney test was used in the case of a non-Gaussian distribution. GraphPad Prism was used to determine the statistical significance. Results represent means ± SEM. Differences were considered significant at a *$p<0.05$, **$p<0.01$ or ***$p<0.001$.

Results

Synthesis and characterization of PAA-AgNPs. AgNPs with sizes of 30 nm and 45 nm were prepared by adapting the modified Tollens process using PAA at different concentrations and maltose as a reducing agent. In the case of reduction using $NaBH_4$, AgNPs with an average size of 10 nm were prepared (Figure 1A). The average particle size of AgNPs prepared at different concentrations of PAA and with different reducing agents in the reaction system was monitored by DLS and by recording the absorption spectra. The size of the prepared NPs was subsequently confirmed by electron microscopy. PAA proved to be a very effective tool for controlling the size of the prepared silver NPs reduced by maltose, even at very low PAA concentrations, as published in earlier work [23]. In the absence of PAA, the reaction yielded AgNPs with an average size of 28 nm. In the presence of PAA at a very low concentration of 10^{-10} mol/l, the average size increased only slightly to 30 nm (Figure 1B). Such an extremely low concentration of PAA has only a minimal impact on the final size of the AgNPs. In the case of a higher PAA concentration of 2.5×10^{-9} mol/l, larger particles were prepared with an average size of 45 nm (Figure 1C). The changes in the sizes of the prepared AgNPs depending on the concentration of PAA and the type of reducing agent in the reaction system are also reflected in their optical properties. In the absorption spectra, there was a shift of the surface plasmon maxima towards higher wavelengths (Figure 1D). The surface plasmon of spherical AgNPs with a mean size of 10 nm is localized at 396 nm and shifts towards 411 nm and 423 nm for nanoparticles of 30 nm and 45 nm, respectively, with increasing nanoparticle size.

10 nm but not 30 nm or 45 nm PAA-AgNPs inhibit cell growth of A549 and HEL299 cells. To analyze the cytotoxic effects associated with the size of PAA-AgNPs (10 nm, 30 nm, and 45 nm Ag core), cell viability was determined in lung cancer cell line A549 and lung fibroblast non-cancer cell line HEL299 following 24 h exposure. PAA-AgNPs(10) lowered the viability of A549 cells at 6.3 μg/ml and the highest concentration of 50 μg/ml showed an almost 100% decrease (Figure 2A). The viability of HEL299 cells was decreased by about 50% already at 3.1 μg/ml, with 12.5 μg/ml and higher concentrations of PAA-AgNPs being detrimental for the cells (Figure 2A). PAA-AgNPs(30) and PAA-AgNPs(45) did not affect dramatically the cell viability of either, HEL299 and A549 cells (Figure 2A). Therefore, for the next experiments, concentrations up to 5 μg/ml PAA-AgNPs were chosen to analyze the biological effects of the three types of nanoparticles. At first, the proliferation activity of A549 cells was estimated for 48 h revealing the marked inhibition of growth by PAA-AgNPs(10) compared to 30 nm and 45 nm nanoparticles (Figure 2B). As visible from the confluency

Table 1. Primer sequences used for qRT-PCR analyses.

gene	primer	sequence (5'→3')
TNFA	forward	TGGAGAAGGGTGACCGACTC
Tumor necrosis factor alpha	reverse	TCCTCACAGGGCAATGATCC
IL-10	forward	CTTCCATTCCAAGCCTGACC
Interleukin 10	reverse	CCCAAGCCCAGAGACAAGATAA
SOD1	forward	CATTGCATCATTGGCCGCACACTG
Superoxide dismutase 1	reverse	GGCGATCCCAATTACACCACAAGC
FN1	forward	AAGACCAGCAGAGGCATAAG
Fibronectin	reverse	CCAACGGCATAATGGGAAAC
POLR2A	forward	GCACCACGTCCAATGACAT
RNA polymerase II subunit A	reverse	GTGCGGCTGCTTCCATAA

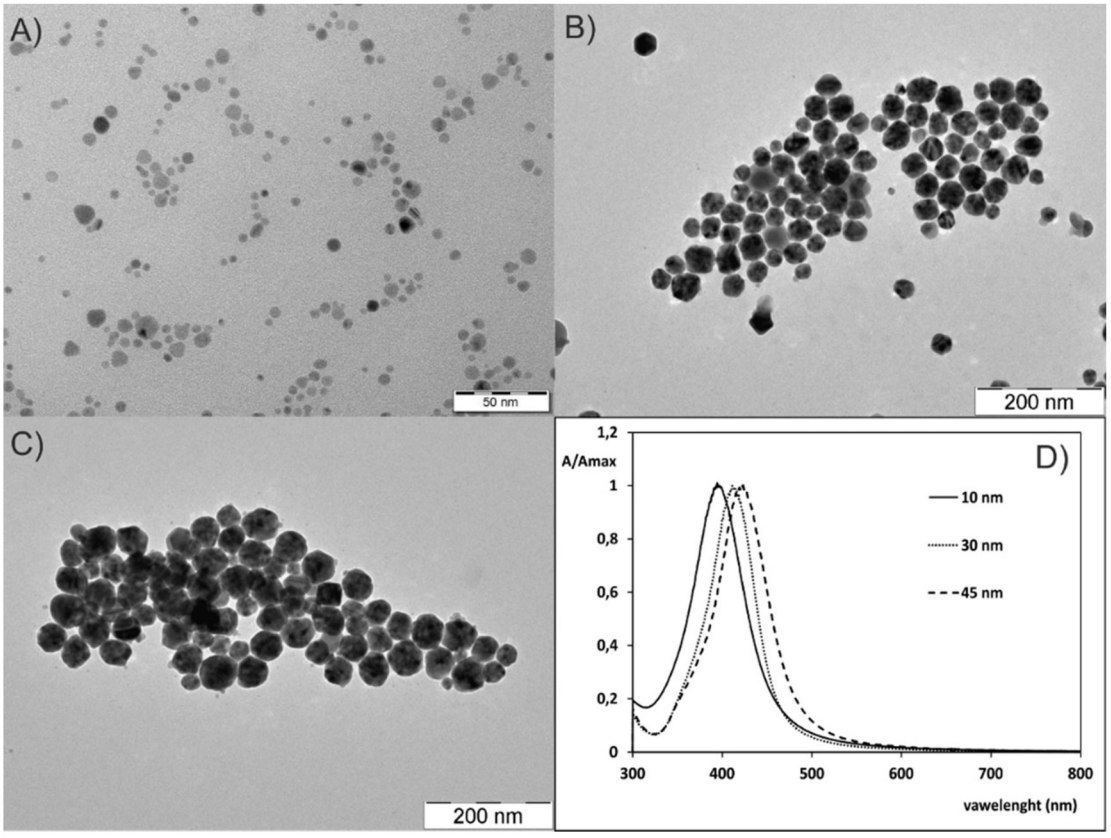

Figure 1. Characterization of PAA-AgNPs. Electron microscopy images of PAA-AgNPs reduced by A) NaBH4 at 2.5×10^{-9} mol/ PAA, B) maltose at 10^{-10} mol/ PAA, C) maltose at 2.5×10^{-9} PAA, and D) corresponding absorption spectra of prepared PAA-AgNPs dispersions with various sizes.

mask images, the cells were viable but did not proliferate in the presence of PAA-AgNPs(10) (Figure 2B). Unlike A549 cells, HEL299 cells represent normal lung fibroblasts growing naturally slower than cancer cells. To analyze the growth till 80% confluency as in the case of A549, the initial density of HEL299 cells was set to 40% (toward 20% in A549 cells). Similarly, as in the case of A549, PAA-AgNPs(10) retarded the growth of HEL299 cells, while the nanoparticles of bigger sizes had no effect on proliferation (Figure 2C).

PAA-AgNPs(10) induce apoptosis and changes in the cell cycle in A549 and HEL299 cells. To understand the results from the proliferation assay, the cell cycle of A549 cells after the incubation with PAA-AgNPs was determined. As expected, the exposure to PAA-AgNPs(10) was associated with a smaller proportion of A549 cells in the G1 phase and a bigger proportion in the G2 phase when higher (4 and 5 μg/ml) concentrations were used (Figures 3A, 3C; Supplementary Figure S1A). No changes in the cell cycle of A549 cells were detected after incubation with PAA-AgNPs(30) or PAA-AgNPs(45) (Figure 3A; Supplementary Figures S1A, S1C). Whether or not the G2/M arrest observed with PAA-AgNPs(10) might have been associated with the induction of apoptosis in A549 cells was further investigated by the analysis of annexin V. Flow cytometry for annexin V revealed that indeed, A549 cells exposed to PAA-AgNPs(10) for 24 h showed a higher rate of apoptosis (Figures 3B, 3D; Supplementary Figure S1B). No degree of apoptosis was detected after the exposure to PAA-AgNPs(30), and with 5 μg/ml of PAA-AgNPs(45) a low number of apoptotic cells was detected (Figure 3B; Supplementary Figures S1B, S1D). Accordingly, the cell cycle was determined in HEL299 cells after exposure to PAA-AgNPs. Already 3 μg/ml of PAA-AgNPs(10) was responsible for the decline of cell proportion in the G1 phase and the increase in S and G2 phases in HEL299 cells (Figure 4A; Supplementary Figure S2A). Interestingly, a concentration of 5 μg/ml PAA-AgNPs(10) (already highly toxic for HEL299 as shown in Figure 4A) caused an opposite effect, an increase in the G1 and a reduction in the S phases (Figure 4A; Supplementary Figure S2A). Additionally, there was a population of aneuploid cells detected at this highest concentration reaching almost 45%, observed mostly in the G1 phase (Figure 4C). Also, in HEL299 cells, the G2/M arrest caused by PAA-AgNPs(10) has been linked to apoptosis as 4 μg/ml and 5 μg/ml concentrations caused a dramatic increase in apoptotic cells (Figures 4B, 4D; Supplementary Figure S2B). Incubation with PAA-AgNPs(30)

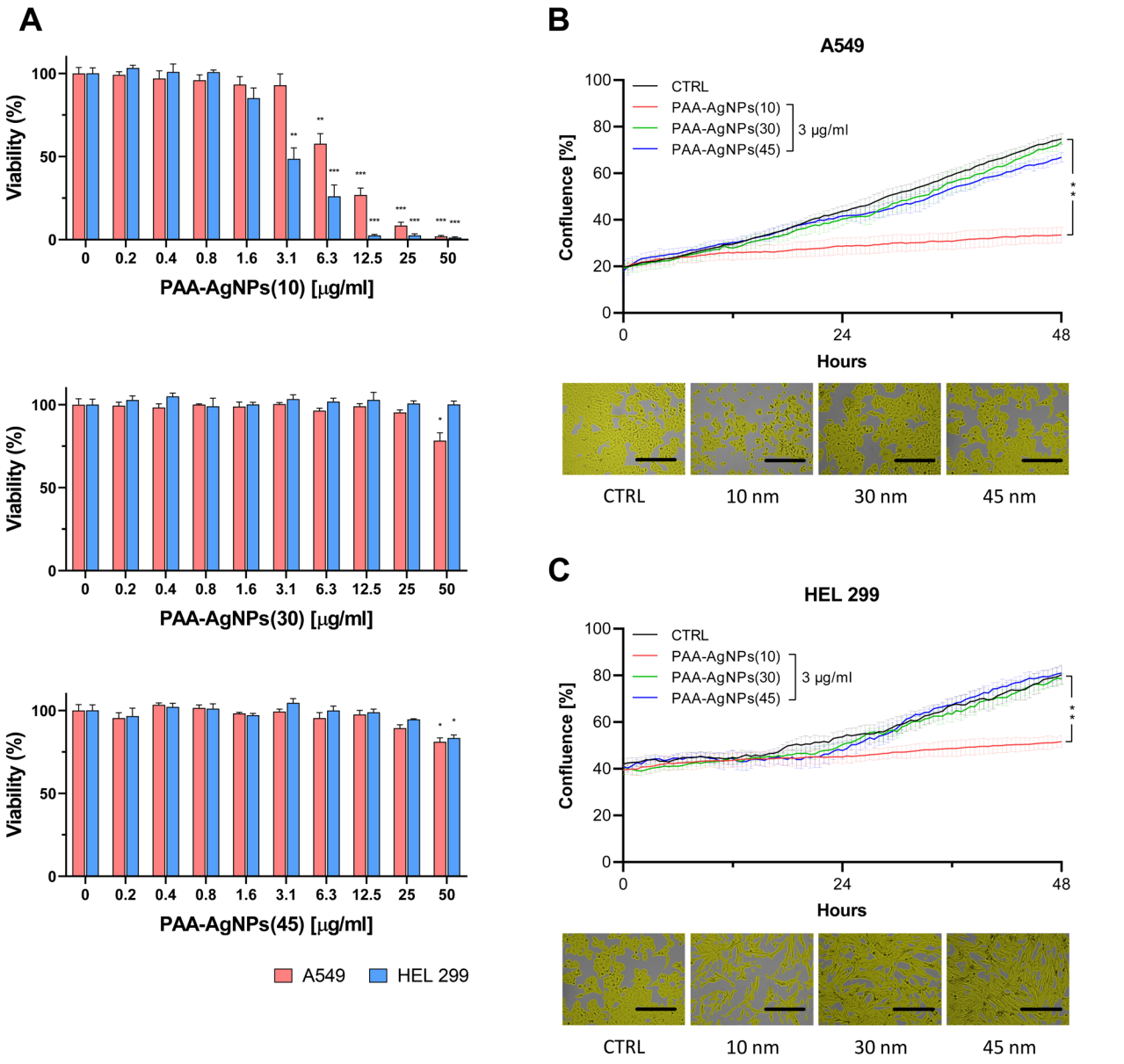

Figure 2. A) Cytotoxicity of PAA-AgNPs in A549 and HEL299 cells. Cytotoxicity was determined by MTT assay shown as a percentage of viable cells after 24 h exposure with defined extracellular concentrations of nanoparticles. The proliferation of A549 (B) and HEL299 (C) cell lines treated with PAA-AgNPs for 48 h. The bottom panels of images show the confluency mask. The scale bar represents 500 μm. The data are given as means ± SEM from the three independent experiments. *p<0.05, **p<0.01, and ***p<0.001 vs. a non-exposed control

and PAA-AgNPs(45) led to no visible changes in cell cycle progression or apoptosis induction in HEL299 cells (Figures 4A, 4B; Supplementary Figures S2A–S2D).

PAA-AgNPs-induced mRNA shows a different pattern for each size of the silver core. In addition to apoptosis and cell cycle changes caused by PAA-AgNPs, changes in mRNA expression induced by nanoparticle presence have been estimated in A549 and HEL299 cells. qRT-PCR results showed that PAA-AgNPs are able to induce an inflammatory response in both, A549 and HEL299 cells, however following different expression patterns in regard to the size of the silver core. PAA-AgNPs(10) induced the strongest *TNFA* response from the three types of AgNPs which was followed by an increase in its anti-inflammatory counterpart *IL-10* in A549 cells (Figure 5A). PAA-AgNPs(10) also increased the level of *FN1* mRNA and *SOD1* mRNA (Figure 5A). Expression patterns of mRNAs induced by PAA-AgNPs(30) were much weaker. *TNFA* and *IL-10* mRNA showed a minimal increase, while *FN1* and *SOD1* were unchanged (Figure 5B). PAA-AgNPs(45) predominantly activated the synthesis

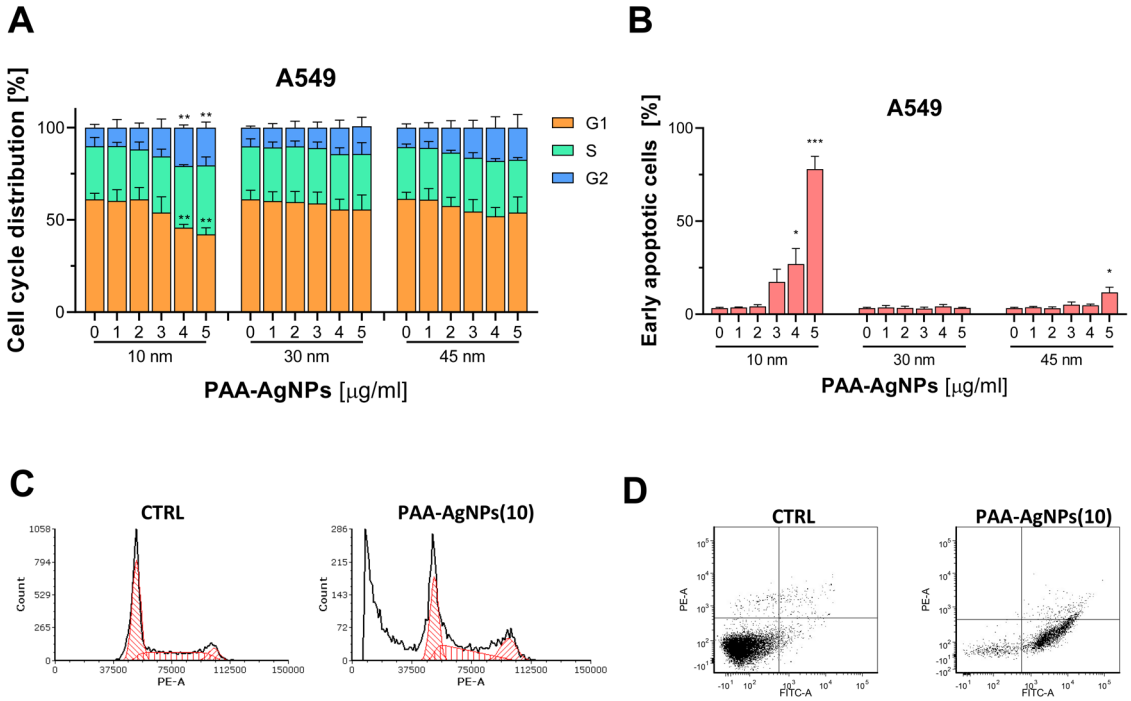

Figure 3. Cell cycle and apoptosis detection in A549 cells. Cell cycle (A) and apoptosis (B) analyses of A549 cells treated with PAA-AgNPs determined by flow cytometry shown as a percentage of cells after 24 h exposure with defined extracellular concentrations of nanoparticles. Cell distribution in the phases of the cell cycle shown for 5 μg/ml PAA-AgNPs(10) (C). An early apoptosis detection using annexin V shown in cells treated with 5 μg/ml PAA-AgNPs(10) (D). The data are given as means ± SEM from the three independent experiments. *p<0.05, **p<0.01, and ***p<0.001 vs. a non-exposed control

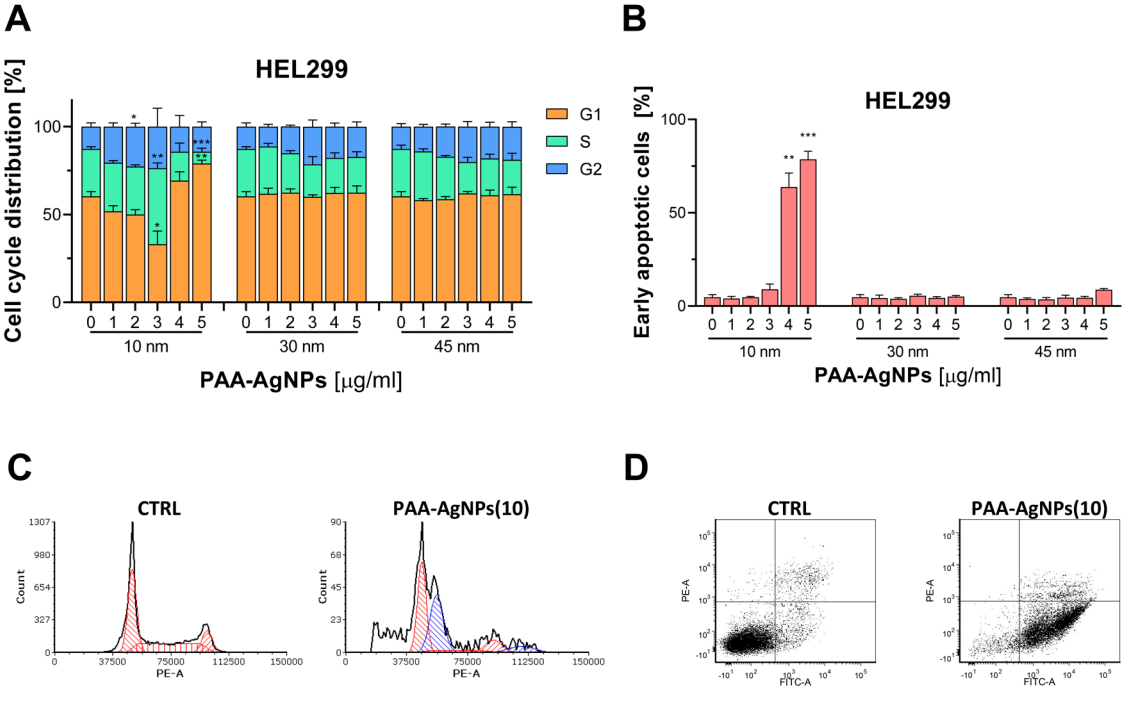

Figure 4. Cell cycle and apoptosis detection in HEL299 cells. Cell cycle analysis (A) and apoptosis (B) of HEL299 cells treated with PAA-AgNPs determined by flow cytometry shown as a percentage of cells after 24 h exposure with defined extracellular concentrations of nanoparticles. Cell distribution of diploid cells (red) and aneuploid cells (blue) in the phases of the cell cycle shown for 5 μg/ml PAA-AgNPs(10) (C). An early apoptosis detection using annexin V shown in cells treated with 5 μg/ml PAA-AgNPs(10) (D). The data are given as means ± SEM from the three independent experiments. *p<0.05, **p<0.01, and ***p<0.001 vs. a non-exposed control

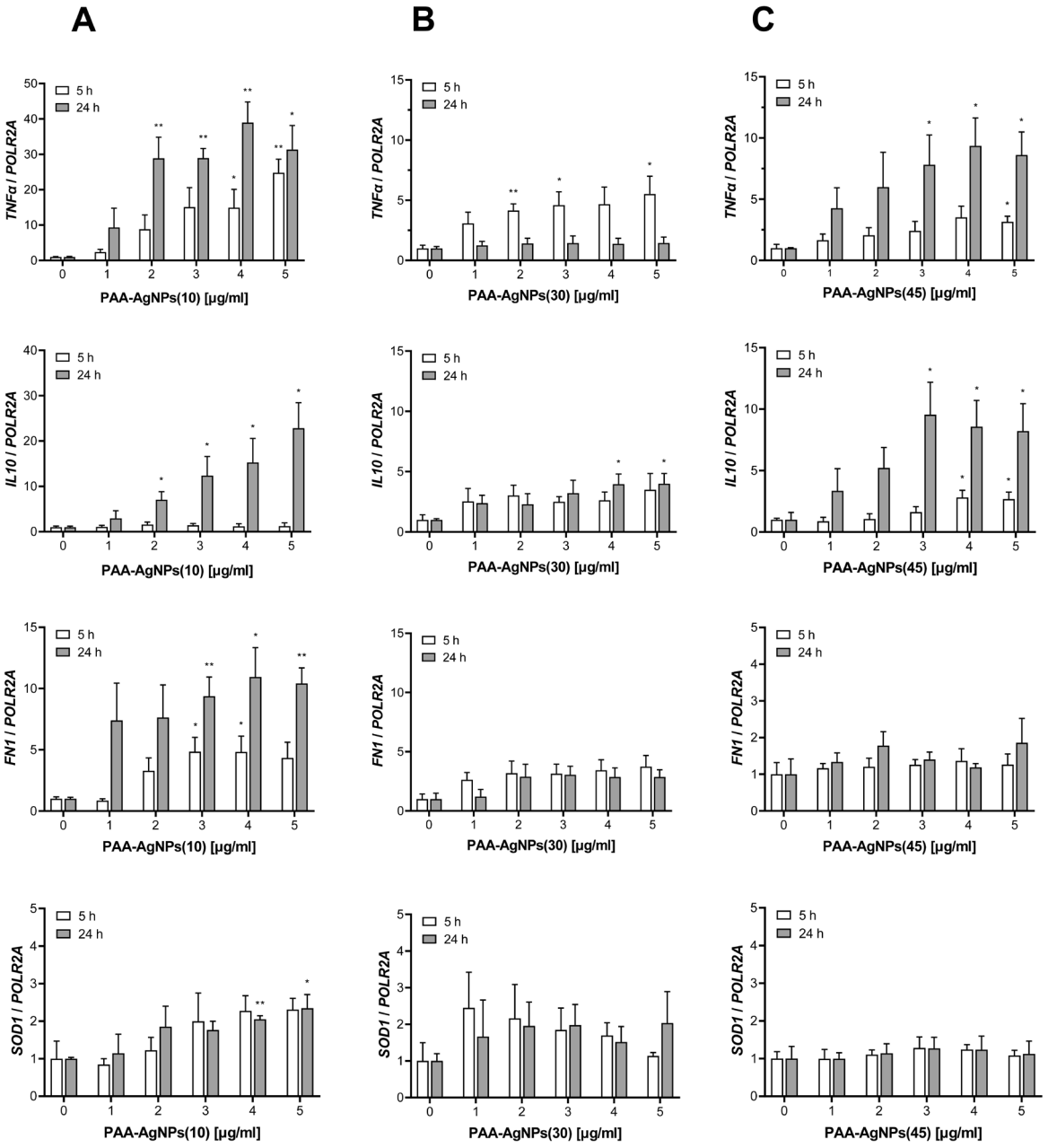

Figure 5. PAA-AgNP-induced genes in A549 cells, qRT-PCR for *TNFA*, *IL-10*, *FN1*, and *SOD1* in A549 cells after the short- (5 h) and long-term (24 h) exposure with defined extracellular concentrations of PAA-AgNPs(10) (A), PAA-AgNPs(30) (B), and PAA-AgNPs(45) (C). The data are given as means ± SEM from the three independent experiments. *p<0.05, **p<0.01, and ***p<0.001 vs. a non-exposed control

of *TNFA* and *IL-10* mRNA in longer time-point with no change in *FN1* and *SOD1* (Figure 5C). In HEL299 cells, PAA-AgNPs(10) induced a much stronger inflammatory response with high levels of *TNFA* and *IL-10* mRNA already 5 h after treatment compared to A549 cells (Figure 6A). Interestingly, no increase in *FN1* and *SOD1* mRNA was measured (Figure 6A). Similarly, no induction of *FN1* and *SOD1* has been detected after exposure to PAA-AgNPs(30) and PAA-AgNPs(45), and only a mild increase in *TNFA* mRNA was observed (Figure 6B). Only PAA-AgNPs(45) incubation lead to the synthesis of *IL-10* mRNA (Figure 6C).

PAA-AgNPs induce cell cytoskeleton changes in A549 as well as in HEL299 cells. Apart from the changes occurring at the molecular level, the alterations in cell structural properties induced by PAA-AgNPs in A549 (Figure 7A) and HEL299 (Figure 7E) cells were investigated. Interestingly,

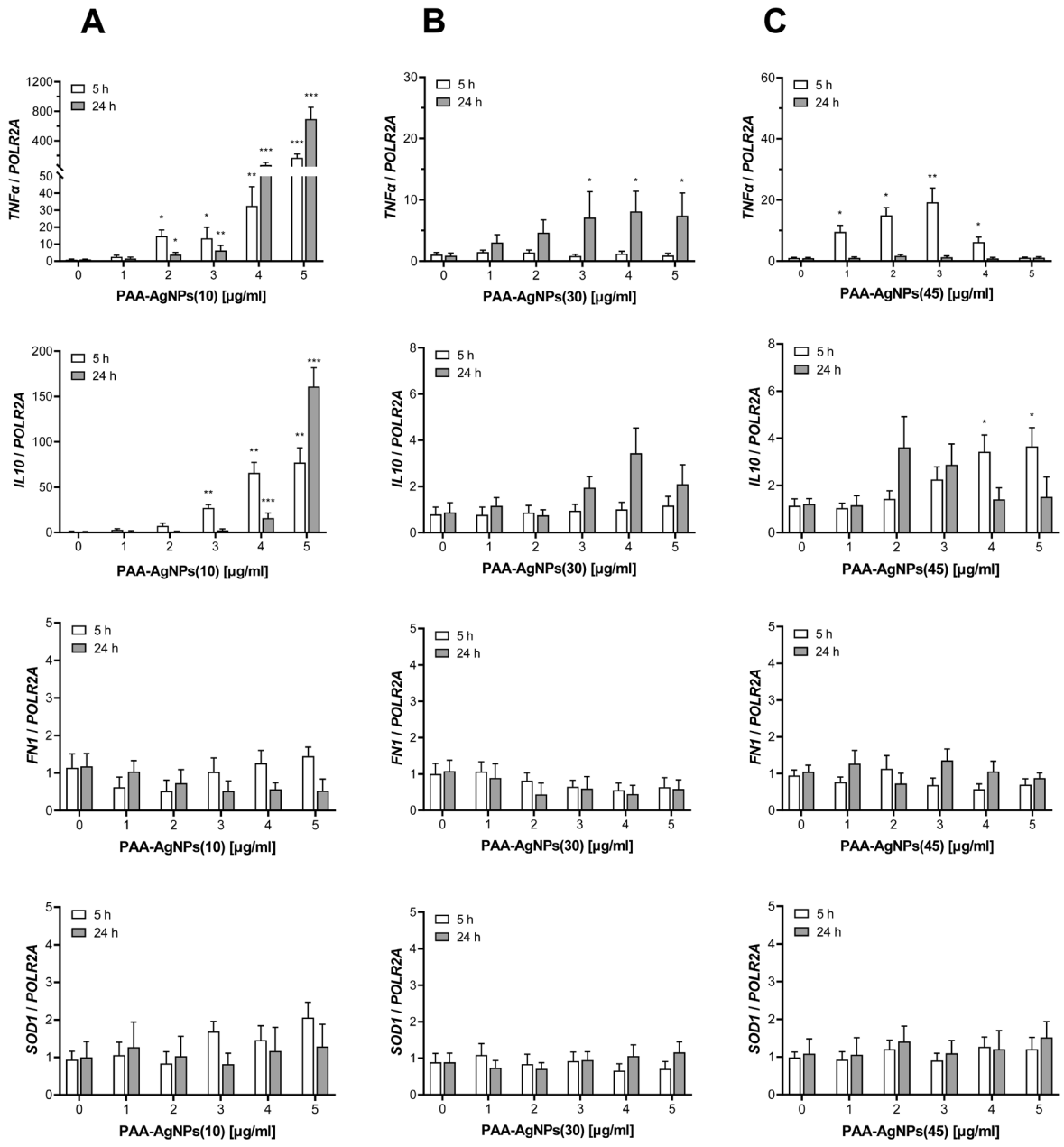

Figure 6. PAA-AgNP-induced genes in HEL299 cells, qRT-PCR for *TNFA*, *IL-10*, *FN1*, and *SOD1* in HEL299 cells after the short- (5 h) and long-term (24 h) exposure with defined extracellular concentrations of PAA-AgNPs(10) (A), PAA-AgNPs(30) (B), and PAA-AgNPs(45) (C). The data are given as means ± SEM from the three independent experiments. *p<0.05, **p<0.01, and ***p<0.001 vs. a non-exposed control

PAA-AgNPs(10) caused the strongest actin cytoskeleton remodeling effects in both, A549 as well as HEL299 cells. PAA-AgNPs(10) at 5 µg/ml initiated redistribution of actin filaments and stress fibers in A549 cells after 24 h (Figure 7B), while it caused actin cytoskeleton rearrangement and formation of large intracellular actin-rich vesicles in HEL299 cells (Figure 7F). Incubation of A549 cells with 5 µg/ml PAA-AgNPs(30) resulted in a marked disruption of actin cytoskeleton structure with F-actin visible in separate clusters rather than filaments (Figure 7C), and in HEL299 cells actin depolymerization has been observed with complete disappearance of F-actin assembly (Figure 7G). Treatment of A549 cells with 5 µg/ml PAA-AgNPs(45) led to similar changes as observed for 30 nm nanoparticles (Figure 7D), nevertheless, the same nanoparticles led to no visible F-actin alterations in HEL299 cells (Figure 7H).

Discussion

Nanomaterials with antimicrobial properties have been suggested as an alternative to traditional antibiotics, especially noble metal nanoparticles like AgNPs [17]. Despite the reported cytotoxicity of AgNPs in lung cancer cells A549, as well as other cancer cell lines, they are considered promising therapeutic agents against cancer [24, 25]. In our study, we focused on AgNPs-induced biological effects not only in cancer A549 cells but also in normal lung fibroblast HEL299 cells to understand how biologically effective doses of AgNPs that can potentially lead to the elimination of lung tumor tissue may affect non-cancer neighboring lung tissue. For the purpose of this study, we used a previously published modified Tollens reduction method for the preparation of AgNPs with different sizes in order to evaluate the biological effects of AgNPs depending on the particle size. PAA-coated nanoparticles with three sizes of the silver core (10 nm, 30 nm, 45 nm) were incubated with both types of cells to compare their impact on viability, cell cycle progression, apoptosis, mRNA induction, and cytoskeletal remodeling. Size is usually not considered a factor that may lead to the striking toxicological impact of particles at the large scale, however, our results show that by certain types of nanoparticles, such as PAA-AgNPs, the size of metal core might have a substantial impact on nanoparticle cytotoxicity. The impact of PAA-AgNPs(10) on cells proved to be the strongest of the three nanoparticle types, dramatically reducing cell growth when compared to bigger nanoparticle types. Considerable dose-dependent inhibition of A549 cell proliferation in response to AgNPs which was shown previously [22], was confirmed in our study for PAA-AgNPs(10) not only in the case of A549 but also in non-cancer HEL299 cells. The cell cycle analysis revealed a lower proportion of cells in the G1 phase indicating the cell cycle arrest in the G2/M checkpoint in A549 as well as HEL299 cells treated with higher concentrations of PAA-AgNPs(10). These results correlate with other data showing AgNPs causing cell cycle arrest in the G2/M phase [26–28]. Results of cell cycle estimation in HEL299 cells showing a dramatic increase of cell number in the G1 phase and a dramatic decrease in S and G2 phases after exposure to 5 μg/ml PAA-AgNPs(10) was at least partially caused by the formation of aneuploidy. Such genotoxic effect of the AgNPs resulting in aneuploidy has been previously shown [28–31]. Whether or not these cell cycle alterations were associated with the induction of apoptosis was further analyzed. Higher concentrations of PAA-AgNPs(10) led to an increase in apoptotic cell numbers in A549 as well as HEL299 cells. PAA-AgNPs(30) neither affected viability nor initiated apoptosis in both cell types. PAA-AgNPs(45) increased the number of apoptotic A549 cells only with the highest concentration used, while no apoptosis induction for HEL299 cells was measured. This is an interesting

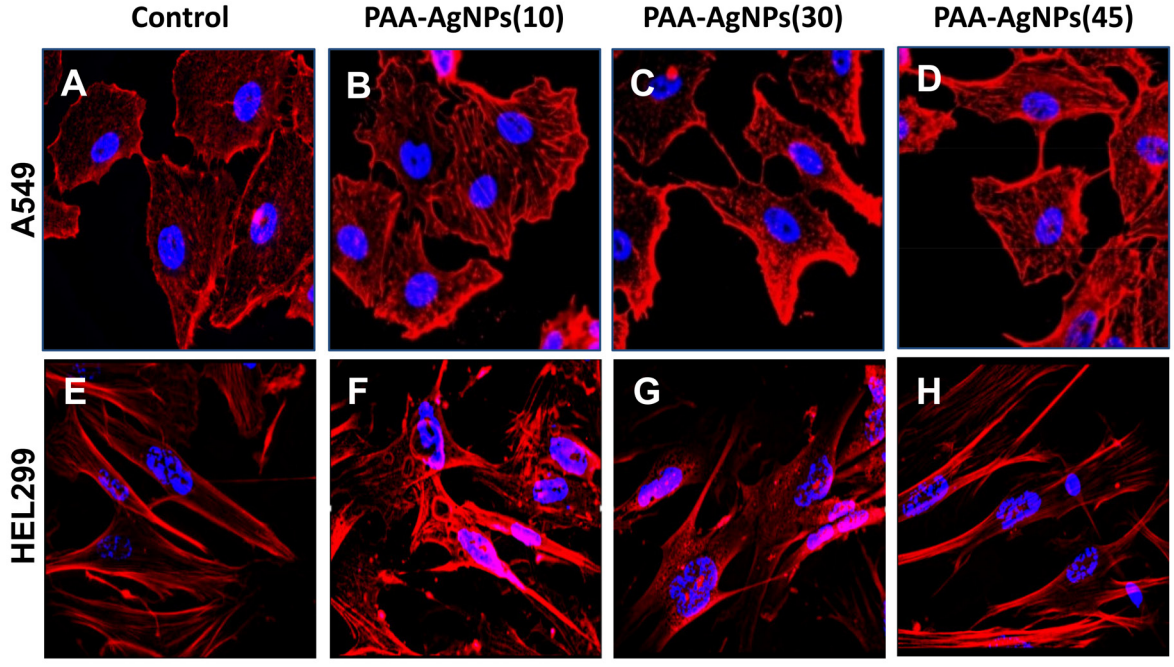

Figure 7. Changes in the cytoskeleton of A549 and HEL299 cells caused by PAA-AgNPs. Immunofluorescence showing PAA-AgNPs core size-dependent remodeling of the actin cytoskeleton in A549 and HEL299 cells. Phalloidin staining of the actin cytoskeleton in A549 (A–D) and HEL299 (E–H) cells with 5 μg/ml PAA-AgNPs for 24 h. Notes: red-phalloidin, blue-DAPI; magnification: 200×

observation, which may point to the potential of this type of PAA-AgNPs to induce apoptosis with higher concentrations in cancer cells, while not affecting (or to a lower degree) the survival of non-cancer cells. Oxidative stress is one of the typical biological effects caused by cell – nanoparticle interaction that may lead to the expression of inflammatory mediators [32]. A549 and HEL299 cells were incubated with PAA-AgNPs for short (5 h) and long (24 h) time points to analyze the induction of mRNA synthesis. PAA-AgNPs(10) were shown to induce early as well as late inflammatory and fibrotic responses. Cells responded strongly to PAA-AgNPs(10) expressing high *TNFA* mRNA levels in A549 as well as HEL299 cells. This strong proinflammatory reaction led to elevated levels of anti-inflammatory *IL-10* probably in an attempt to temper the inflammatory process. Interestingly, the responses to PAA-AgNPs(30) and PAA-AgNPs(45) were rather moderate with *TNFA* and *IL-10* much lower than in the case of PAA-AgNPs(10) in A549 as well as HEL299 cells. Fibrotic tissue damage is another reported endpoint following nanoparticle deposition in lung cells [33]. Physical and chemical properties of nanomaterials including size, shape, surface modification, and stability importantly contribute to the development of such pathological processes [34]. Fibronectin mRNA was elevated after exposure to PAA-AgNPs(10) in A549 cells. However, no elevation was observed in HEL299 cells with PAA-AgNPs. The lung fibroblast cytoskeletal organization has been shown to be different between normal and fibrotic lung tissue [35]. To determine how PAA-AgNPs may impact cell cytoskeletal structure in A549 as well as in HEL299 cells, the actin cytoskeleton was compared with and without PAA-AgNPs treatment. Incubation of PAA-AgNPs with the cells resulted in actin cytoskeleton remodeling. A comparison of A549 and HEL299 cells revealed that the cytoskeleton stability of cells exposed to PAA-AgNPs is similar between the two cell types. HEL299 cells as typical fibroblasts were flat and possessed a spindle-like shape, whereas A549 cells displayed a cobblestone appearance. PAA-AgNPs(10) showed the most intensive actin cytoskeletal rearrangement involving stress fibers formation in A549 cells and the formation of intracellular actin-rich vesicles in HEL299 cells, which was in line with a strong impact of PAA-AgNPs(10) on the viability and apoptosis of these cells. PAA-AgNPs(30) also induced weaker cytoskeletal remodeling in A549 and HEL299 cells than PAA-AgNPs(10). Interestingly, PAA-AgNPs(45) caused changes in cell cytoskeleton only in A549 cells, whereas they did not affect the cytoskeletal structure of HEL299 cells. This is very interesting, as this with the induction of apoptosis in A549 but not in HEL299 cells points to a certain advantage of PAA-AgNPs(45) affecting more cancer A549 and less not non-cancer HEL299 cells at higher concentrations. Our results suggest that the initiation of inflammatory response in pulmonary cells (cancer and non-cancer) and associated changes in the morphology of these cells represented by actin cytoskeleton remodeling belong to the biological effects caused by AgNPs coated with PAA. From the nanoparticle types tested, PAA-AgNPs(30) and PAA-AgNPs(45) showed fewer undesirable effects on pulmonary cells compared to PAA-AgNPs(10).

The rapid development of nanomaterials engineered for medical purposes brings novel treatment possibilities also into lung disease therapy. Additionally, to all other routes of entering the tissues, nanoparticles may reach lung cells also by inhalation, which on the one hand side may increase the spectrum of therapeutical approaches, on the other hand, it may increase the risk of potential lung tissue damage [36]. Nanoparticle-delivery systems developed to override conventional cancer chemotherapeutics must therefore be carefully checked for their toxicity to become an effective cure for respiratory diseases [37]. The therapeutic potential of PAA-AgNPs in the treatment possibilities of lung cancer has been confirmed by our study and the results suggested that AgNPs like PAA-AgNPs might be considered for cancer chemotherapy. Moreover, we have defined their anti-cancer effects with respect to non-cancer lung cells, something, that is missing in the current literature. Evaluation of anti-cancer effects in comparison to non-cancer cells can help to accelerate safe-by-design approaches in nanomedicine.

Supplementary information is available in the online version of the paper.

Acknowledgments: This study was performed during the implementation of the project Building-up Centre for advanced materials application of the Slovak Academy of Sciences, ITMS project code 313021T081 supported by Research & Innovation Operational Programme funded by ERDF. The authors gratefully acknowledge financial support from the Ministry of Health of the Czech Republic (project NU20-05-00165) and the Internal Student Grant Agency of the Palacký University in Olomouc, Czech Republic (IGA_PrF_2023_024). This work was supported by the Slovak Research and Development Agency under Contract No. APVV-16-0579, and by VEGA grant no. 2/0116/22 and 2/0160/21.

References

[1] MENSAH F, SEYOUM H, MISRA P. Nanomaterials in Nanomedicine, pp 253–277. In: Mistra P. (Eds.) Applied Spectroscopy and the Science of Nanomaterials. Progress in Optical Science and Photonics, vol 2. Springer 2015. https://doi.org/10.1007/978-981-287-242-5_11

[2] ZHANG L, GU FX, CHAN JM, WANG AZ, LANGER RS et al. Nanoparticles in medicine: therapeutic applications and developments. Clin Pharmacol Ther 2008; 83: 761–769. https://doi.org/10.1038/SJ.CLPT.6100400

[3] LI YF, CHEN C. Fate and Toxicity of Metallic and Metal-Containing Nanoparticles for Biomedical Applications. Small 2011; 7: 2965–2980. https://doi.org/10.1002/smll.201101059

[4] SHVEDOVA AA, KISIN ER, MERCER R, MURRAY AR, JOHNSON VJ et al. Unusual inflammatory and fibrogenic pulmonary responses to single-walled carbon nanotubes in mice. Am J Physiol Lung Cell Mol Physiol 2005; 289: L698–708. https://doi.org/10.1152/ajplung.00084.2005

[5] WANG M, LI J, DONG S, CAI X, SIMAITI A et al. Silica nanoparticles induce lung inflammation in mice via ROS/PARP/TRPM2 signaling-mediated lysosome impairment and autophagy dysfunction. Part Fibre Toxicol 2020; 17: 1–22. https://doi.org/10.1186/S12989-020-00353-3/FIGURES/10

[6] ARMSTRONG L, JORDAN N, MILLAR A. Interleukin 10 (IL-10) regulation of tumour necrosis factor alpha (TNF-alpha) from human alveolar macrophages and peripheral blood monocytes. Thorax 1996; 51: 143–149. https://doi.org/10.1136/thx.51.2.143

[7] LEE B, LEE MJ, YUN SJ, KIM K, CHOI IH et al. Silver nanoparticles induce reactive oxygen species-mediated cell cycle delay and synergistic cytotoxicity with 3-bromopyruvate in Candida albicans, but not in Saccharomyces cerevisiae. Int J Nanomedicine 2019; 14: 4801–4816. https://doi.org/10.2147/IJN.S205736

[8] AMEH T, GIBB M, STEVENS D, PRADHAN SH, BRASWELL E et al. Silver and Copper Nanoparticles Induce Oxidative Stress in Bacteria and Mammalian Cells. Nanomaterials (Basel) 2022; 12: 2402. https://doi.org/10.3390/nano12142402

[9] DĄBROWSKA-BOUTA B, SULKOWSKI G, STRUŻYŃSKI W, STRUŻYŃSKA L. Prolonged Exposure to Silver Nanoparticles Results in Oxidative Stress in Cerebral Myelin. Neurotox Res 2019; 35: 495–504. https://doi.org/10.1007/s12640-018-9977-0

[10] KENYON NJ, BRATT JM, LEE J, LUO J, FRANZI LM et al. Self-Assembling Nanoparticles Containing Dexamethasone as a Novel Therapy in Allergic Airways Inflammation. PLoS One 2013; 8: e77730. https://doi.org/10.1371/JOURNAL.PONE.0077730

[11] KAMAT CD, SHMUELI RB, CONNIS N, RUDIN CM, GREEN JJ et al. Poly(beta-amino ester) nanoparticle-delivery of p53 has activity against small cell lung cancer in vitro and in vivo. Mol Cancer Ther 2013; 12: 405. https://doi.org/10.1158/1535-7163.MCT-12-0956

[12] YAMADA M, FOOTE M, PROW TW. Therapeutic gold, silver, and platinum nanoparticles. Wiley Interdiscip Rev Nanomed Nanobiotechnol 2015; 7: 428–445. https://doi.org/10.1002/wnan.1322

[13] SIDDIQI KS, HUSEN A, RAO RAK. A review on biosynthesis of silver nanoparticles and their biocidal properties. J Nanobiotechnology 2018; 16: 14. https://doi.org/10.1186/S12951-018-0334-5

[14] MARAMBIO-JONES C, HOEK EMV. A review of the antibacterial effects of silver nanomaterials and potential implications for human health and the environment. Journal of Nanoparticle Research 2010; 12: 1531–1551. https://doi.org/10.1007/S11051-010-9900-Y

[15] MILLER CN, NEWALL N, KAPP SE, LEWIN G, KARIMI L et al. A randomized-controlled trial comparing cadexomer iodine and nanocrystalline silver on the healing of leg ulcers. Wound Repair Regen 2010; 18: 359–367. https://doi.org/10.1111/J.1524-475X.2010.00603.X

[16] GALIANO K, PLEIFER C, ENGELHARDT K, BRÖSSNER G, LACKNER P et al. Silver segregation and bacterial growth of intraventricular catheters impregnated with silver nanoparticles in cerebrospinal fluid drainages. Neurol Res 2008; 30: 285–287. https://doi.org/10.1179/016164107X229902

[17] YAQOOB AA, AHMAD H, PARVEEN T, AHMAD A, OVES M et al. Recent Advances in Metal Decorated Nanomaterials and Their Various Biological Applications: A Review. Front Chem 2020; 8: 341. https://doi.org/10.3389/fchem.2020.00341

[18] LIU J, ZHAO Y, GUO Q, WANG Z, WANG H et al. TAT-modified nanosilver for combating multidrug-resistant cancer. Biomaterials 2012; 33: 6155–6161. https://doi.org/10.1016/j.biomaterials.2012.05.035

[19] SKIRTACH AG, ANTIPOV AA, SHCHUKIN DG, SUKHORUKOV GB. Remote activation of capsules containing Ag nanoparticles and IR dye by laser light. Langmuir 2004; 20: 6988–6992. https://doi.org/10.1021/la048873k

[20] MUSSA FARKHANI S, ASOUDEH FARD A, ZAKERI-MILANI P, SHAHBAZI MOJARRAD J, VALIZADEH H. Enhancing antitumor activity of silver nanoparticles by modification with cell-penetrating peptides. Artif Cells Nanomed Biotechnol 2017; 45: 1029–1035. https://doi.org/10.1080/21691401.2016.1200059

[21] HE Y, DU Z, MA S, LIU Y, LI D et al. Effects of green-synthesized silver nanoparticles on lung cancer cells in vitro and grown as xenograft tumors in vivo. Int J Nanomedicine 2016; 11: 1879–1887. https://doi.org/10.2147/IJN.S103695

[22] JAGTAP RR, GARUD A, PURANIK SS, RUDRAPAL M, ANSARI MA et al. Biofabrication of Silver Nanoparticles (AgNPs) Using Embelin for Effective Therapeutic Management of Lung Cancer. Front Nutr 2022; 9: 1465. https://doi.org/10.3389/fnut.2022.960674

[23] PANÁČEK A, PRUCEK R, HRBÁČ J, NEVEČNÁ T, ŠTEFFKOVÁ J et al. Polyacrylate-assisted size control of silver nanoparticles and their catalytic activity. Chem Mater 2014; 26: 1332–1339. https://doi.org/10.1021/cm400635z

[24] GENGAN RM, ANAND K, PHULUKDAREE A, CHUTURGOON A. A549 lung cell line activity of biosynthesized silver nanoparticles using Albizia adianthifolia leaf. Colloids Surf B Biointerfaces 2013; 105: 87–91. https://doi.org/10.1016/j.colsurfb.2012.12.044

[25] JEYARAJ M, SATHISHKUMAR G, SIVANANDHAN G, MUBARAKALI D, RAJESH M et al. Biogenic silver nanoparticles for cancer treatment: An experimental report. Colloids Surf B Biointerfaces 2013; 106: 86–92. https://doi.org/10.1016/j.colsurfb.2013.01.027

[26] KANIPANDIAN N, LI D, KANNAN S. Induction of intrinsic apoptotic signaling pathway in A549 lung cancer cells using silver nanoparticles from Gossypium hirsutum and evaluation of in vivo toxicity. Biotechnol Rep (Amst) 2019; 23: e00339. https://doi.org/10.1016/j.btre.2019.e00339

[27] HOLMILA RJ, VANCE SA, KING SB, TSANG AW, SINGH R et al. Silver Nanoparticles Induce Mitochondrial Protein Oxidation in Lung Cells Impacting Cell Cycle and Proliferation. Antioxidants (Basel) 2019; 8: 552. https://doi.org/10.3390/antiox8110552

[28] BOBYK L, TARANTINI A, BEAL D, VERONESI G, KIEFFER I et al. Toxicity and chemical transformation of silver nanoparticles in A549 lung cells: dose-rate-dependent genotoxic impact. Environ Sci Nano 2021; 8: 806–821. https://doi.org/10.1039/D0EN00533A

[29] MUHAMAD M, AB RAHIM N, WAN OMAR WA, NIK MOHAMED KAMAL NNS. Cytotoxicity and Genotoxicity of Biogenic Silver Nanoparticles in A549 and BEAS-2B Cell Lines. Bioinorg Chem Appl 2022; 2022: 8546079. https://doi.org/10.1155/2022/8546079

[30] ASHARANI PV, LOW KAH MUN G, HANDE MP, VALIYAVEETTIL S. Cytotoxicity and Genotoxicity of Silver Nanoparticles in Human Cells. ACS Nano 2009; 3: 279–290. https://doi.org/10.1021/nn800596w

[31] WISE SR JP, GOODALE BC, WISE SS, CRAIG GA, PONGAN AF et al. Silver nanospheres are cytotoxic and genotoxic to fish cells. Aquat Toxicol 2010; 97: 34–41. https://doi.org/10.1016/j.aquatox.2009.11.016

[32] SUN Q, TAN D, ZE Y, SANG X, LIU X et al. Pulmotoxicological effects caused by long-term titanium dioxide nanoparticles exposure in mice. J Hazard Mater 2012; 235–236: 47–53. https://doi.org/10.1016/j.jhazmat.2012.05.072

[33] CHO WS, DUFFIN R, POLAND CA, DUSCHL A, OOSTINGH GJ et al. Differential pro-inflammatory effects of metal oxide nanoparticles and their soluble ions in vitro and in vivo; zinc and copper nanoparticles, but not their ions, recruit eosinophils to the lungs. Nanotoxicology 2012; 6: 22–35. https://doi.org/10.3109/17435390.2011.552810

[34] TABET L, BUSSY C, SETYAN A, SIMON-DECKERS A, ROSSI MJ et al. Coating carbon nanotubes with a polystyrene-based polymer protects against pulmonary toxicity. Part Fibre Toxicol 2011; 8: 3. https://doi.org/10.1186/1743-8977-8-3

[35] MARINKOVIĆ A, LIU F, TSCHUMPERLIN DJ. Matrices of physiologic stiffness potently inactivate idiopathic pulmonary fibrosis fibroblasts. Am J Respir Cell Mol Biol 2013; 48: 422–430. https://doi.org/10.1165/rcmb.2012-0335OC

[36] DONALDSON K, POLAND CA. Inhaled nanoparticles and lung cancer – what we can learn from conventional particle toxicology. Swiss Med Wkly 2012; 142: w13547. https://doi.org/10.4414/smw.2012.13547

[37] DA SILVA AL, SANTOS RS, XISTO DG, DEL V ALONSO S, MORALES MM et al. Nanoparticle-based therapy for respiratory diseases. An Acad Bras Cienc 2013; 85: 137–146. https://doi.org/10.1590/s0001-37652013005000018

https://doi.org/10.4149/neo_2023_230525N283

Effects of different-sized silver nanoparticles on morphological and functional alterations in lung cancer and non-cancer lung cells

Kristina JAKIC[1], Michal SELC[1,2], Radka MACOVA[1], Antonia KURILLOVA[3], Libor KVITEK[3], Ales PANACEK[3,*], Andrea BABELOVA[1,2,*]

Supplementary Information

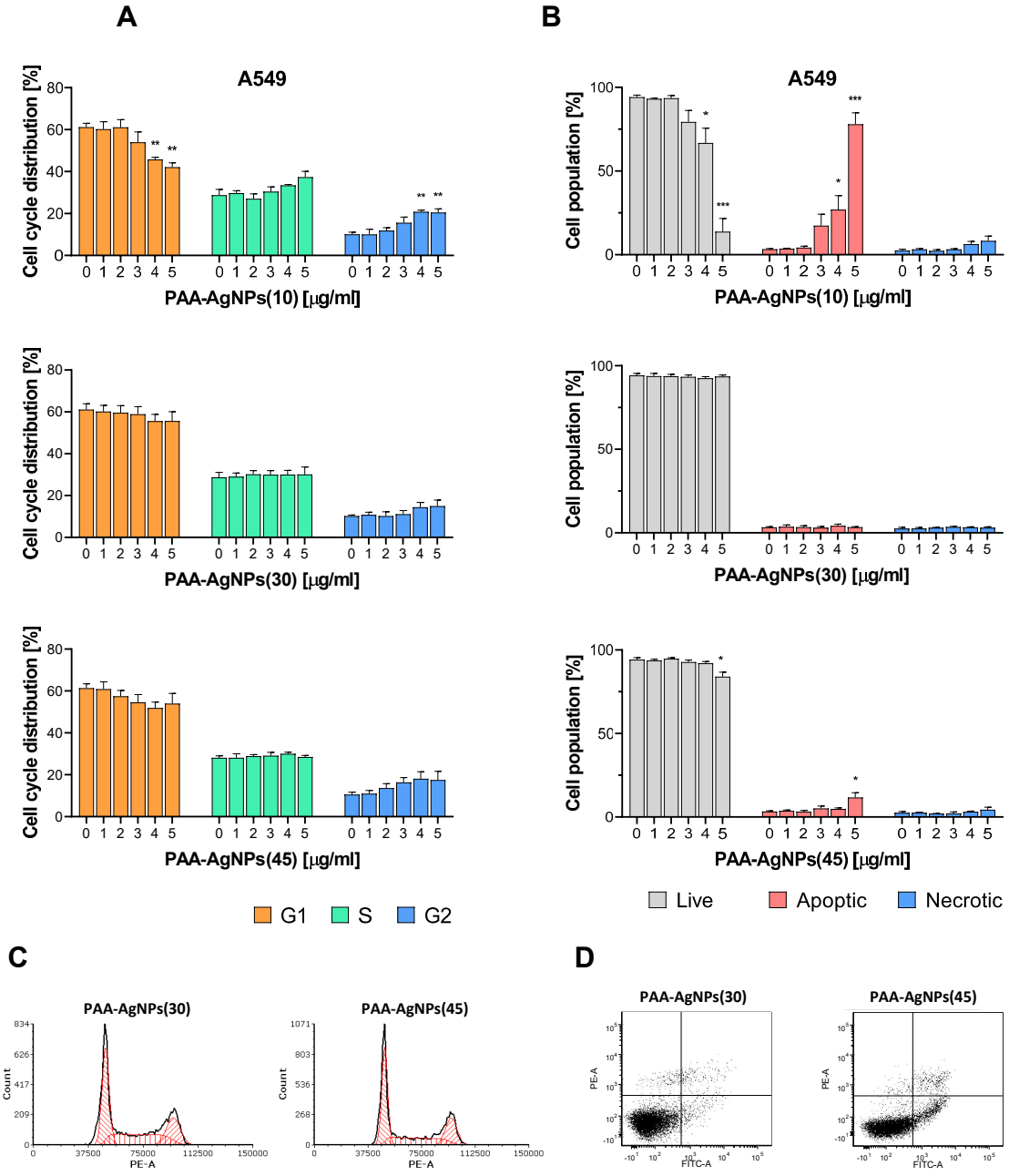

Supplementary Figure S1. Cell cycle and apoptosis detection in A549 cells. Cell cycle (A) and apoptosis (B) analyses of A549 cells treated with PAA-AgNPs determined by flow cytometry shown as percentage of cells after 24 h exposure with defined extracellular concentrations of nanoparticles. Cell distribution in the phases of the cell cycle shown for 5 μg/ml PAA-AgNPs concentration (C). Early apoptosis detection using annexin V shown in cells treated with 5 μg/ml PAA-AgNPs (D). The data are given as means ± SEM from the three independent experiments. *p<0.05, **p<0.01, ***p<0.001 vs. non-exposed control

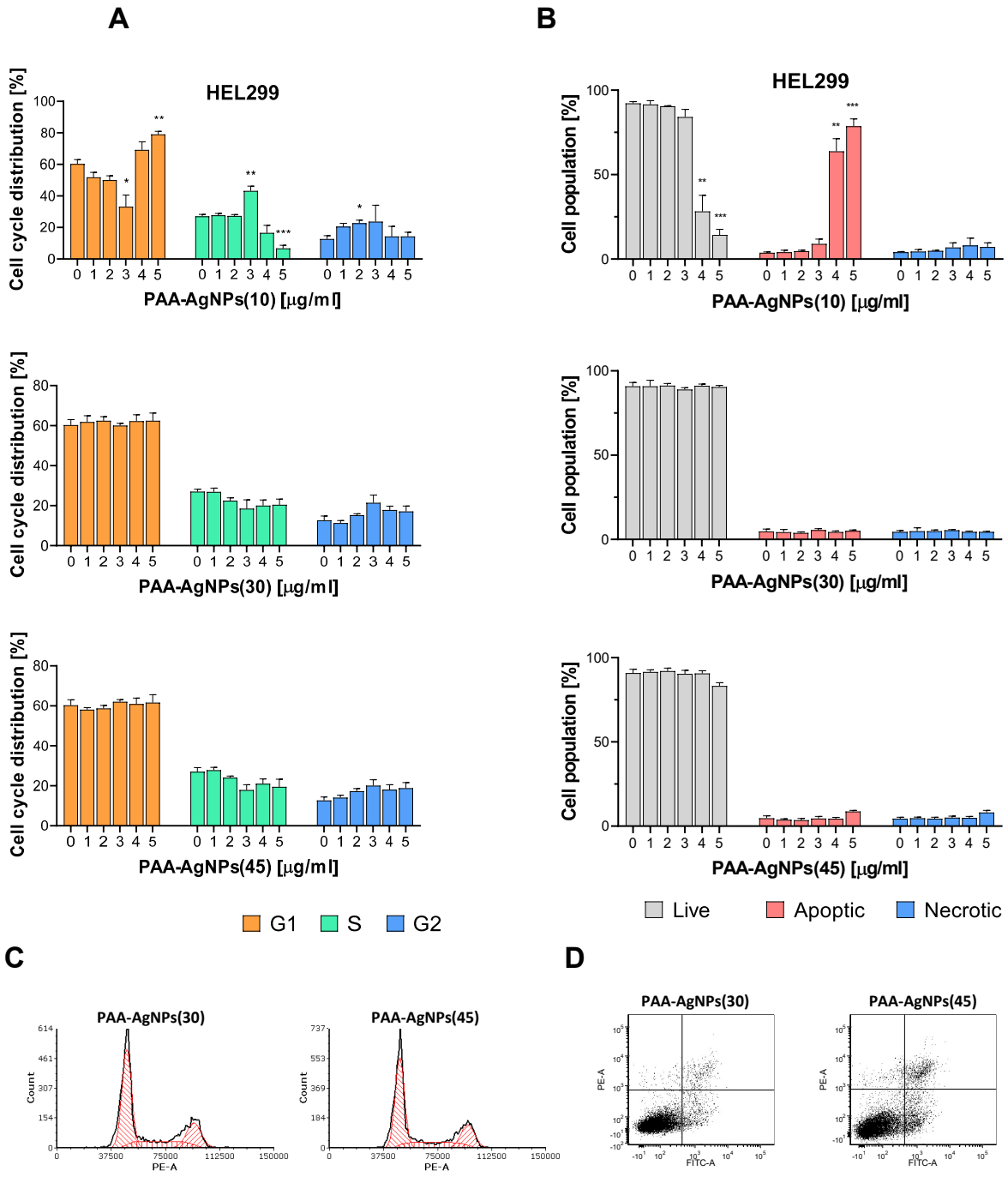

Supplementary Figure S2. Cell cycle and apoptosis detection in HEL299 cells. Cell cycle analysis (A) and apoptosis (B) of HEL299 cells treated with PAA-AgNPs determined by flow cytometry shown as percentage of cells after 24 h exposure with defined extracellular concentrations of nanoparticles. Cell distribution in the phases of the cell cycle shown for 5 μg/ml PAA-AgNPs concentration (C). Early apoptosis detection using annexin V shown in cells treated with 5 μg/ml PAA-AgNPs (D). The data are given as means ± SEM from the three independent experiments. *p<0.05, **p<0.01, ***p<0.001 vs. non-exposed control